On the pre-treatment for recycling spent NdFeB permanent magnets: from disassembling, characterisation to de-coating

Couto, Camila Pucci; van de Ven, Johannes J.M.M.; Yang, Yongxiang; Abrahami, Shoshan T.

DOI
10.1016/j.susmat.2024.e01041

Publication date
2024

Document Version
Final published version

Published in
Sustainable Materials and Technologies

Sustainable Materials and Technologies 41 (2024) e01041

Contents lists available at ScienceDirect

Sustainable Materials and Technologies

journal homepage: www.elsevier.com/locate/susmat

On the pre-treatment for recycling spent NdFeB permanent magnets: from disassembling, characterisation to de-coating

Camila Pucci Couto *, Johannes J.M.M. van de Ven, Yongxiang Yang, Shoshan T. Abrahami

Metals Production Refining and Recycling, Department of Materials Science and Engineering, Faculty of Mechanical Engineering, Delft University of Technology, Mekelweg 2, 2628, CD, Delft, the Netherlands

ARTICLE INFO

Keywords:
NdFeB permanent magnets
Rare-earth elements
Recycling
De-coating
Critical-raw materials

ABSTRACT

An evaluation of neodymium-iron-boron permanent magnets (NdFeB PMs) from different end-of-life products, as a secondary resource of rare-earth elements (REEs), is presented. De-coating of PM was investigate as pre-treatment to facilitate efficient direct magnet recycling. Thus, critical aspects from disassembling to the de-coating of the magnets were addressed. A challenge for the de-coating process is that the magnets have different sizes, weights, and their coating compositions are not known beforehand. It was shown that ammonia-based solutions was thermodynamically suitable to dissolve nickel and zinc coatings selectively, while keeping the bulk magnet stable. Nevertheless, the dissolution of Zn was much faster than the Ni one, and more efficient.

1. Introduction

Critical Raw Materials (CRMs) are classified as the most crucial materials for the European economy, due to their applications in strategic sectors, such as renewable energy, e-mobility, defence, and aerospace [1]. In the 2023 report, the European Commission (EC) has classified 34 raw materials either as critical or strategic, based on their techno-economic importance and supply risk [1,2]. Consequently, the EC has proposed a regulation concerning the supply of CRMs in Europe, in which specific targets must be reached by 2030. Among these targets, it has been established that at least 25% of the European annual consumption of CRMs should come from secondary resources (recycling) [2].

The supply of rare-earth elements (REEs) is considered at the highest risk among the CRMs [1]. The market share of REEs is controlled by China, which has a solid know-how on the extraction of REEs from ores and further processing [3–5]. Thus, China supplies 85–95% of REEs worldwide [5]. Neodymium (Nd) is one of the 17 REEs, with permanent magnet (PM) being its main application as NdFeB alloy, with possible additions of other REEs, such as dysprosium (Dy) and praseodymium (Pr) [3]. PMs can be found, for instance, in hard disk drives (HDDs), smartphones, earbuds, wind turbines, electric and hybrid vehicles [3–8].

Alonso et al. [9] estimated in 2012 that Nd demand would rise by approximately 700% by 2037, driven primarily by the increase in electric vehicles and wind turbines [9]. The Rare Earth Industry Association (REIA) has evaluated the supply of rare-earth oxides (REO); from 2022 to 2033 the supply of REO is expected to increase from 280 kt to over 400 kt [10]. Due to high demand, it is important to ensure a continuous supply of Nd and other REEs. Recycling end-of-life (EoL) products is a feasible alternative to obtain REEs from secondary resources [3,6–8,11–16]. At the same time, it contributes towards achieving the targets proposed by the EC [2].

Currently, approximately 1% of REEs are recovered worldwide from EoL products [1,3,8,17,18], which is far from the 25% EU target [2]. In 2020, it was estimated that approximately 300,000 tons of spent NdFeB PMs were globally stocked as waste electrical and electronic equipment (WEEE) [3], such as computers, smartphones, air conditioners, etc. Since the content of REEs (Nd, Dy, Pr) in the PMs is about 30% [3,6], it means that nearly 89,100 tons of REEs could had been recovered (based on the global estimation from 2020). Therefore, great efforts have been made to develop and/or optimise recycling processes aiming to recover REEs from the spent PMs over the last two decades [3,6,7,11–14,19].

The challenge in the recycling of NdFeB PM is not exclusive to the recovery stage itself; the pre-processing of WEEE is one of the key factors which determines the most suitable recycling route [6,8,15]. The pre-processing consists of multiple steps, mainly sorting, demagnetisation and fragmentation [8]. According to Yang et al. [6] most NdFeB PMs are shredded together with WEEE. Due to their larger size, PMs from electric/ hybrid vehicles and wind turbines, could be pre-dismantled [6]. However, there is no established commercial operation yet; in other

* Corresponding author.
E-mail address: C.PucciCouto@tudelft.nl (C.P. Couto).

https://doi.org/10.1016/j.susmat.2024.e01041
Received 26 February 2024; Received in revised form 5 June 2024; Accepted 5 July 2024
Available online 6 July 2024

words, the pre-dismantling is currently in laboratory/ pilot scale [20]. When PMs are shredded together with WEEE, it results in a heterogeneous (low grade) scrap where different materials are mixed. Therefore, a long recycling route, based either on pyrometallurgical or hydrometallurgical processes, is needed to extract and separate the REEs [8]. However, such long-route processes are associated with extra environmental burden. Pyrometallurgy is based on high temperatures with a high energy consumption, whereas hydrometallurgy consumes large amounts of water and chemical reagents (acid or alkaline solutions) [3,6,7,21,22].

Conversely, a high-grade scrap can be obtained by prior dismantling of EoL to remove the PMs. This results in a concentrated NdFeB scarp that can be processed directly using hydrogen-based methods, such as hydrogen decrepitation (HD), and hydrogenation-disproportionation-desorption-recombination (HDDR). In these methods the brittle magnets are dissociates into coarse hydrogenated granules/powder [6,15,23]. Afterwards, rotation takes place in a porous drum to liberate the hydrogenated NdFeB powder [6]. Thus, it could be used to produce new sintered or bonded permanent magnets [3,15]. These are environmental-friendly methods to recycle PMs, as they only use hydrogen at room temperature and atmospheric pressure [8,15,16,24,25].

One of the challenges in short-route PMs recycling comes from the presence of various protective coatings [26]. Due to the high reactivity of REEs, the NdFeB alloy is prone to corrosion [26–28]. Thus, different types of coatings, either metallics or polymerics, are applied to avoid oxidation of the magnets during their lifespan [14,15,26]. Among the metallic coatings, nickel, nickel-copper-nickel, and zinc are the main systems applied onto PMs [26]. However, the presence of coating influences the direct recycling process. First, the coatings might act as a physical barrier for hydrogen to access the bulk magnet, depending on how dense it is [26,29]. Thus, the magnet bulk must be accessible to guarantee contact between hydrogen gas and the magnet [15,30]. Secondly, the presence of metallic contaminates in the NdFeB powder can have a detrimental impact on the properties of the recycled PM [26,28,29].

The influence of Zn on the magnetic properties of NdFeB has been investigated since the early 2000's [31–37]. Hu et al. [31] showed that NdFeB magnet properties slightly decreases after coating the substrate with Zn. This was attributed to the Zn diffusion along the grain boundaries, and further formation of Nd-Fe-Zn by the consumption of the hard magnet phase $Nd_2Fe_{14}B$ [31]. On the other hand, Lv et al. [37] have found that both magnetic coercivity and remanence are improved, but the Curie temperature slightly decreases with the addition of 2 wt% of Zn in Dy-free NdFeB powders produced by HDDR technology. Horikawa et al. [38] investigated the magnetic properties (remanence and coercivity) of NdFeB PM produced by means of re-sintering fine powders of NdFeB. The powder was coated by sorption treatment with metal vapor, using either Zn, Mg or Yb. Regarding Zn, its detrimental effect on the magnetic properties was attributed to the formation of α-Fe, as a result of the reacting between Zn and Fe from the $Nd_2Fe_{14}B$ matrix. In addition to that, Zn can evaporate during the sintering process of NdFeB [29], which may contaminate the sintering equipment as well.

The effect of Ni on the magnetic properties of NdFeB PMs has not been extensively investigated as the Zn one. Cui et al. [39] have evaluated the effect of Ni powder as an intergranular additive in the composition of NdFeB. According to their findings, both remanence and maximum energy product decrease with increasing in Ni content (0.1–1 wt%). However, the maximum value for intrinsic coercivity was reached with 0.3 wt% of Ni in the composition, but the intrinsic coercivity decreased with Ni content higher than 0.3 wt%. The changes in the microstructure, due to Ni addition, is seen by the formation of Nd(Fe,Ni)B phase. Ni diffuses into the magnetic matrix and replaces the Fe atoms.

Considering the different influences that contamination from metallic coating may have on the magnetic properties of NdFeB, the de-coating can be considered an important pre-treatment of the magnet scrap. One of the first studies focused on this challenge was published by Orefice et al. [28]. The authors evaluated the removal of Ni-Cu-Ni coating from PMs using a mixture of bromine in organic solvents. According to their study, a high coating dissolution yield ($\geq$ 85%) was reached by soaking the samples in solutions of 1% vol bromine containing either ethanol or dimethylformamide. According to visual inspection, the coating was completely dissolved within 1 h [28]. However, the main drawback from this study is the toxicity of dimethylformamide and the use of organic solvents. Furthermore, there is a need to evaluate the dissolution behaviour of other prevalent coating systems present on PMs, such as Zn, which are increasingly present in different EoL magnets. Considering the two most popular metallic coatings for PMs, Ni coating can still be mechanically separated post-treatment. Ni metallic coatings are ductile, forming Ni flakes after hydrogen decrepitation, which can be separated from the powdered NdFeB matrix by sieving [6,15]. However, Grau et al. [29] have reported that this separation of Ni-based coatings as flakes and the HPMS powders is not an easy process; the separation results in a low yield due to a similarity in particle sizes. Regarding Zn, it cannot be separated by sieving because it forms a fine powder after hydrogen decrepitation, which contaminates the NdFeB powder [29]. Hence, the recommendations for Zn-based coatings were either sandblasting or grinding prior to hydrogenation [29].

To enhance the purity of recycled magnets by direct recycling methods, the main objective of this study is to establish a de-coating process as a potential but important pre-treatment step of PM for direct recycling. In addition to that, this work addresses the challenges related to the dismantling of EoL products to retrieve the magnet samples. The samples were characterised according to the magnet type and coating system. Then, only magnets from HDDs and *E*-scooter rotor were used for the de-coating experiments, due to the availability of multiple similar samples. De-coating in ammonia-based solutions was chosen due to its well-known selective leaching of various non-ferrous metals, being suitable for both Ni and Zn metallic coatings [40–43]. This results in the formation of stable ammine complexes for both Ni and Zn, facilitating their selective dissolution over e.g. metallic iron [40,42–44]. In addition to that, the solution presents low toxicity, low cost, and enables a close-loop process due to its easy regeneration [40].

2. Experimental

2.1. Magnets removal and demagnetisation

Samples of PMs were removed manually from different EoL components, including: approximately 40 hard-disc drivers (HDDs), 4 wireless earbuds, 1 electrical toothbrush, 1 speaker from portable sound system, 3 *E*-scooter rotors and 1 electric vehicle rotor. Moreover, 4 samples of PMs from wind turbines and 2 samples from air-conditioners were received for characterisation. Some of these samples were provided by the companies SUEZ (France) and CRM (Belgium). After collecting the samples, the PMs were thermally demagnetised at 400 °C for 1 h. It is important to highlight that the removal of magnets from *E*-scooter and electrical vehicle rotor, was only possible after their demagnetisation, because of both strong magnetism and the presence of glue.

2.2. Characterisation

After demagnetisation, the elemental composition of the bulk magnets was first analysed by X-ray fluorescence (XRF). To obtain an average composition of PMs from HDDs, three different samples from three different HDDs, were milled together. The same procedure was performed for samples from an *E*-scooter rotor; however, all the magnets were from the same rotor. The XRF measurements were carried out with a Panalytical Axios Max WD-XRF spectrometer, and data analysis was performed with SuperQ5.0i/Omnian software.

The chemical composition of the powdered samples from both HDDs

and *E*-scooter were also determined by inductively coupled plasma optical emission spectroscopy (ICP-OES). For doing that, 1 g of powder sample (the same powder characterised by XRF) was dissolved in 100 mL of aqua regia solution (HCl (37%): HNO_3 (65%) = 3:1, *v*/v) at 70 °C for 5 h. At the end of the dissolution, the leachate was diluted with demiwater, and three samples of 10 mL each were analysed by ICP-OES.

Finally, the samples' morphology and coatings thicknesses were analysed by scanning electron microscopy (SEM). Before the microscopic characterisation, the samples were cut-off, mounted in hot resin, ground and polished. SEM images were obtained in secondary electron (SE) and backscattering (BSE) modes. The semi-quantitative elemental characterisation, and the mappings of the chemical composition were undertaken by energy dispersive X-ray spectroscopy (EDS). The microscope was set to operate with acceleration voltage of 20 kV, probe current of 60 pA, and working distance between 10 and 12 mm.

2.3. De-coating

For selective dissolution of their coating layers, NdFeB PMs removed from HDDs and an *E*-scooter were used. The chosen PMs from HDDs and E-scooter had an average weight of 6 and 7 g, respectively). Two different ammonia-based solutions were used. The first one consisted of 5 M NH_3 with the addition of 0.25 M NH_4Cl (1:1 *v*/v), whereas the second solution used was 5 M NH_3 with addition of HCl (37% v/v) to adjust the pH to 9. The concentration and chosen salt addition was selected based on preliminary tests.

The experimental set-up consisted of a 500 mL three-neck flask placed in a water bath at constant temperature of 75 °C. A condenser, where cooling water ran during the experiment, was attached to the flask. 300 mL of solution was used for each dissolution experiment. The solid-liquid ratio was not considered, due to the differences in size and weight of magnets.

The coating dissolution was monitored for 5–6 h; every hour a liquid sample from the leachate (5 mL) was withdrawn for ICP-OES analysis. This was done to determine the coating-dissolution rate. At the end of the experiment, the bulk sample was characterised either by XRF or SEM-EDS.

In addition to the experimental work, the thermodynamic aspects of metals dissolution in NH_3 were evaluated by calculating *E*-pH diagrams and reactions using the HSC software (version 10.1.0.1). The overview of the experimental workflow is given in Fig. 1. All bulk magnets were characterised by XRF and SEM-EDS, but only samples from HDDs and *E*-scooter had a more detailed elemental characterisation. The main reason for this choice was related to the availability of multiple similar samples. The average chemical composition of samples from either HDDs or *E*-scooter was determined by XRF and ICP-OES using a powder consisting of different samples, as explained in the section 2.2. Finally, only samples of HDDs and E-scooter were experimentally studied for de-coating in ammonia-based solutions.

3. Results and discussion

3.1. Liberation and demagnetisation

The manual dismantling of HDDs, speakers, toothbrush, and earbuds was relatively easy and possible without demagnetisation. However, this process is time-consuming, mainly for non-trained operators. As an example, the disassembling of a single HDD may take 10–15 min. On the other hand, PMs from the rotors of *E*-scooter and E-vehicle were tightly embedded (and possibly glued), so that they could only be removed after thermal demagnetisation.

The Curie temperature for NdFeB alloy is 312 °C [7]. However, if Pr or Dy are present in the alloy's composition, the Curie temperature is typically higher and could reach 400 °C [4,7,8]. For this reason, all samples were submitted to a thermal demagnetisation at 400 °C for 1 h. Most of the samples were successfully demagnetised, except the magnets present in the speaker and in the toothbrush. The fact that some magnets did not demagnetise at the established condition (400 °C for 1 h), indicates that, possibly, the magnets' chemical composition is not NdFeB, and the Curie temperature should be higher than 400 °C. Ferrite magnets (also known as M-type), for instance, present Curie temperature of 450 °C [45]. Therefore, these samples were heated again up to 500 °C for 1 h. After that, all the samples were completely demagnetised.

Fig. 2 shows examples of samples which were disassembled, and then characterised. In general, the PMs vary in terms of shape, size and weight. The average value of the dimensions from the samples analysed, are summarised in Table 1. The design of the electric vehicle rotor (Fig. 2 (a)) consists of a layered structure of electric steel, and the magnets are arranged as a dodecahedron. This complex design makes manual liberation of PMs from such product challenging. In total, there are 20 magnets in the electric vehicle rotor shown in Fig. 2 (a). However, because the complete disassembly and removal of the magnets was not possible, the weight and the dimensions were not measured. For the purpose of this work, some layers of the steel plates were manually removed, and small pieces of magnets were cut-off with a manual drill machine for the characterisation of the magnets. In that way, it was possible to estimate the length (10 mm) and thickness (4 mm) of the magnets. In contrast, after demagnetisation, the *E*-scooter rotor (Fig. 2 (b)) was easily opened and the magnets could be taken out from the inside. There were about 40 magnets, in a rectangle shape of approximately 7 g each, with a height of 18 mm.

The quantity, size and weight of PMs from HDDs varied according to the type and size of the HDD, the brand and the production year. Some examples are shown in Fig. 2 (c) indicating the difference in size of typical HDD PMs. As an example, the weight of 14 PMs from different HDDs varied between 1.4 and 23.36 g. In general, old HDDs (early 2000s) have only one large and heavy (>10 g) PM, whereas the ones manufactured after 2005 have usually 2 smaller and lighter PMs. Moreover, the thickness may differ substantially from 0.5 to 2 mm. Detailed information about the HDDs used can be found in the Supplementary data (Table S1).

In the rotor of an electric toothbrush (Fig. 2(d)) 2 PMs were found;

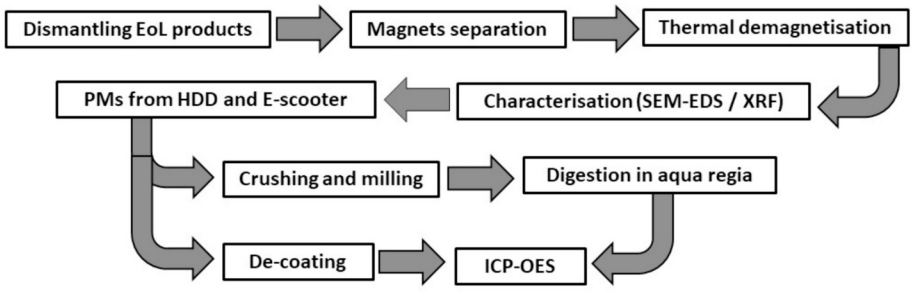

Fig. 1. Overview highlighting the main steps of the experimental workflow.

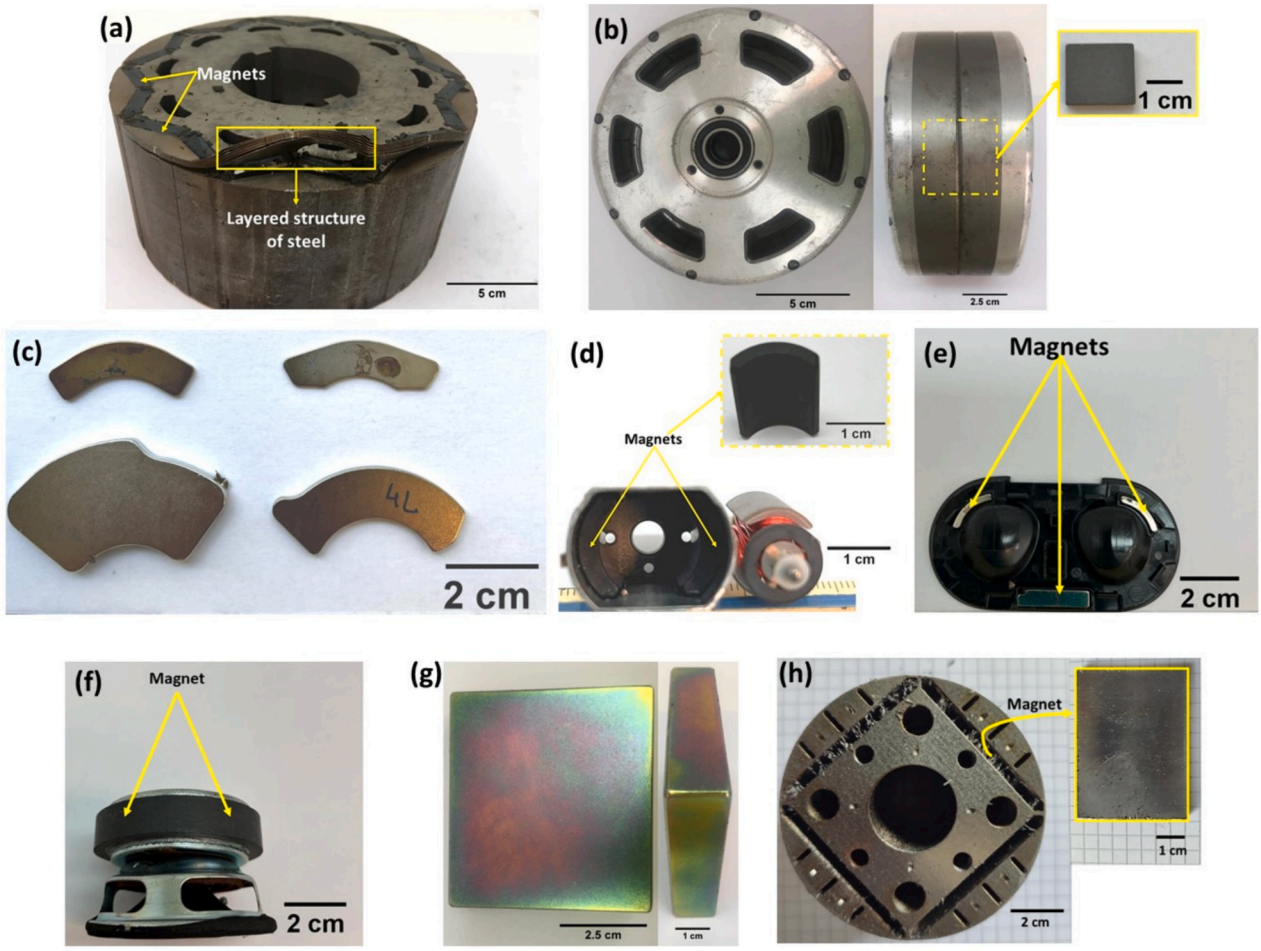

Fig. 2. Examples of magnets from different end-of-life products, such as: (a) electric vehicle; (b)*E*-scooter; (c) HDDs; (d) electric tooth brush; (e) earbuds; (f) speaker; (g) wind turbine; (h) air conditioner.

Table 1
- Summary of the dimensions and the weight of different NdFeB PM characterised samples.

EoL product	Average dimensions [*h* x *l* x *w*] [1] (mm)	Weight (g)	Total amount of magnets	Total weight (g)
Air conditioner	40 × 30 × 1	4	4	16
Earbuds	2 × 5 × 0.5	0.05–0.5	5	0.7
E-scooter	18 × 16 × 1	7	40	280
Electric toothbrush	18 × 12 × 1	4	2	8
Electric vehicle	Not measured	Not measured	20	1500–2500 [2]
HDD	5 × 30 × 1	1–23	1–2	2–23 [3]
Speakers	$d^* = 50$ mm / $w = 8$ mm	73	2	146
Wind turbine	60 × 52 × 13	330	N.A. [4]	80–650 Kg/MW [4]

[1] h: height / l: length / w: width / d: diameter.
[2] References values obtained from [20].
[3] Usually, HDDs with lighter PMs have at least two PMs. It is hard to estimate the total amount or weight of PMs in HDDs.
[4] The quantity of PMs in wind turbines varies greatly. The total weight is represented as kg/MW with reports ranging from 80 to 650 Kg/MW [46].

they have a concave shape with height of 18 mm, and weight of 4.05 g each. Conversely, an earbud may be composed of several small PMs as seen in Fig. 2(e). Their weight can vary from 0.05 g to 0.5 g. The dimension of the smaller one is 2 mm in length and <1 mm in width and height, whereas the larger one has an area of 10 mm^2 and is <1 mm thick. On the other hand, the PM from speaker has a shape of a ring, as shown in Fig. 2(f); it shows 50 mm diameter, 73.44 g in weight and thickness of 8 mm.

The samples of PMs from wind-turbine and air-conditioner rotors, shown in Fig. 2 (g) and Fig. 2 (h) respectively, were received already disassembled. The ones analysed from wind turbines are 13 mm thick, with an average weight of 330 g. Regarding the rotor from an air conditioner, the quantity of PMs may vary. The one characterised (Fig. 2 (g)) had 4 PMs in a rectangular shape, each of them approximately 40 mm high and weighing 4.05 g.

It is important to highlight that the samples shown in Fig. 2 are just examples. As mentioned before, the characteristics of PMs may change over the years, as well as according to their producers and applications. For instance, another rotor from *E*-scooter consists of 60 magnets, with different dimensions (23 × 10 × 1) mm, and an average weight of 6.4 g in comparison with the ones seen in Fig. 2 (b).

From the disassembly step it is already possible to consider some

challenges regarding the recycling of the PMs. The manual dismantling is the most effective way to obtain high-grade of PM scraps to be directly recycled. That would be more suitable for the *E*-scooter, wind turbines and HDDs, although the latter is very labour intensive. On the other hand, small magnets such as the ones from earbuds, cannot be easily liberated and produce too low yield to justify the efforts. Overall, due to the complex design of these products this step is time-consuming and not efficient. On the other hand, automatic dismantling has been shown as an alternative to manual dismantling, which guarantees obtaining high-grade scrap with less labour/ time-consuming [23].

3.2. Chemical composition

To confirm whether all magnets were NdFeB-type, and identify the type of coating for further characterisation of its morphology, preliminary elemental characterisation of the PM samples was carried out by both XRF and SEM-EDS. These characterisation results are combined and summarised in Table 2.

From the 8 different types of applications that were analysed, only two magnets were not composed of NdFeB: the ones found in the speaker and the electric toothbrush. Magnets from the electric toothbrush were identified as strontium ferrite (SrFeO), whereas the magnets from speakers were a barium ferrite (BaFeO).

Regarding the NdFeB PMs evaluated in this study, the most commonly applied metallic coatings are Zn or Ni, despite nearly 15 possible reported coatings for NdFeB PM [26]. The PMs from HDDs were all coated with Ni, whereas magnets from *E*-scooter, wind turbine, and air conditioner had a protective layer of Zn. The magnet samples from earbuds had either Ni-Cu-Ni or Zn metallic coating. Non-metallic coatings, such as epoxy, can also be found as a protective layer for PMs, for instance in wind turbines and in the electric-vehicle rotor. Furthermore, not all PMs from the air conditioner had a coating layer; some of them appeared to be non-coated.

For a quantitative elemental analysis of the chemical composition of the coated NdFeB PMs, ICP-OES measurements were carried out on 1 g of powdered samples of PMs either from HDDs or from an *E*-scooter dissolved in aqua regia. As mentioned before, these magnets were selected due to the availability of multiple similar samples, to determine the average chemical composition as shown in Table 3.

The ICP-OES results of crushed and milled samples in Table 3 show a substantial contrast in the coatings' content of the two different analysed PMs samples. The Ni content in HDD-magnets is about 7 wt%, while in PMs from an E-scooter the average amount of Zn is much lower, only 0.4 wt%. Regarding REEs, the Nd content is the highest in the NdFeB alloy. Moreover, 1.3% of Dy is seen in the PMs for both applications (HDDs and E-scooter). Dy is often added to improve the resistance to temperature and demagnetisation [47]. Nevertheless, the composition of the PMs from the E-scooter rotor is clearly different from the HDDs. Namely, the total concentration of REEs is higher due to the addition of other REEs, such as Pr, Gd and Ho. These elements enhance specific properties and help reduce raw materials costs, for instance: Gd increases the thermal stability, and Ho improves corrosion and mechanical properties [6,48]. All REEs have been classified at high-critical supply risk according to EU [1]. Hence, the recycling of PMs not only represent an alternative source for Nd supply, but also for other REEs. On the other hand, this raises technological challenges related to the separation of these REEs during the recycling process.

3.3. Coatings characterisation

Visual inspection of the samples after dismantling and after demagnetisation revealed, in general, great damage to the coating layers and consequently, the exposure of the NdFeB substrate. Two examples are given in Supplementary data - Fig. S1. Different reasons contributed to that: use of sharp tools (screw drivers) to liberate the magnets, adhesion with glue, and the effect of high temperature from the demagnetisation step. The latter can promote superficial cracks in the coating layer, resulting in its peeling off. It was mostly seen in PMs coated with Zn. However, two different Zn coatings were found among the samples analysed; they are named as “blue” and “colour” [26]. The blue one was found in PMs from *E*-scooter (Fig. 2(b)), while the Zn-colour coating was seen in PMs from wind turbine (Fig. 2 (g)). It was the Zn-colour coating more prone to damage after demagnetisation. Additionally, Ni coating in PMs from HDDs was also easily peeling off after the thermal treatment.

The cross-sections of metallic-coated NdFeB PMs were characterised by SEM-EDS, to evaluate the thickness and morphology of the coating layers. Fig. 3 shows the cross-sections of PMs from different EoL products: (a) E-scooter, (b) wind turbine, (c) air conditioner, and (d) earbud. Based on SEM images (Fig. 3), the bulk morphology and composition of the samples are similar, consisting of a Fe—Nd matrix with Nd-rich phase randomly distributed, in accordance with literature [26,27]. However, the thickness of the coating layer varies among these samples. The PM from wind turbine (Fig. 3 (b)) shows the thickest coating layer (≈ 80 μm), while the PM from air conditioner (Fig. 3 (c)) are the thinnest ones (≈ 4 μm). The thickness of the coating might be correlated to the application of the PM. It is expected that a wind turbine will have to operate for 20 to 40 years [49] under a range of (severe) environmental conditions, considering that wind turbines can be found both on-shore and off-shore. Therefore, a thick zinc coating layer is desired in such applications. This agrees with the findings of Durodola et al. [50] which have investigated the influence of different electroplating parameters on the corrosion resistance of Zn plated mild steels. The authors showed better corrosion resistance for samples with higher Zn content, and thicker coating layer. On the other hand, the lifetime of an air conditioner, for instance, varies from 10 to 15 years and it is exposed to much less severe environments, which justifies the application of a thin coating layer.

In Fig. 4, the cross-sections of PMs from three different HDDs are shown. The samples were produced in different years (2001, 2006 and 2007). Their bulk morphology does not differ much from other samples, as seen in Fig. 3. However, large cracks can be observed in Fig. 4 (b) and Fig. 4 (c). This can be attributed to the preparation of thin samples for SEM analysis; procedures such as griding and polishing may break the bulk magnet, due to its brittle characteristic [7]. Nevertheless, the thickness of the coating layer varies among the samples, although to a less degree compared to samples in Fig. 3. The oldest sample, from 2001 (Fig. 4(a)), has the thicker coating layer (≈ 20 μm), while the newest,

Table 2
- Summary of XRF and SEM-EDS characterisation of bulk and coating composition of magnets from different EoL products.

EoL product	Number of available EoL products	Number of magnets characterised	Type of magnet	Coating system
Air conditioner	2	2	**NdFeB**	**Zn** or none
Earbuds	4	2	**NdFeB**	**Ni-Cu-Ni**
E-scooter	3	8	**NdFeB**	**Zn**
Electric toothbrush	1	1	SrFeO	None
Electric vehicle	1	1	**NdFeB**	Epoxy
HDD	70	12	**NdFeB**	**Ni**
Speakers	2	1	BaFeO	None
Wind turbine	2	2	**NdFeB**	**Zn** or epoxy

Table 3
- Elemental composition (wt%) of NdFeB PM from HDD and *E*-scooter determined by ICP-OES analyses.

Composition of EoL PM	Fe	Nd	Ni	Pr	Dy	Gd	B	Co	Ho	Al	Zn	Others*
HDD	69.9	19.9	6.7	–	1.3	–	0.9	0.5	–	0.4	–	0.2
E-scooter	73.2	16.6	–	3.5	1.3	1.2	1.1	1.0	0.7	0.6	0.4	0.3

* Cu, Na, S, Zr.

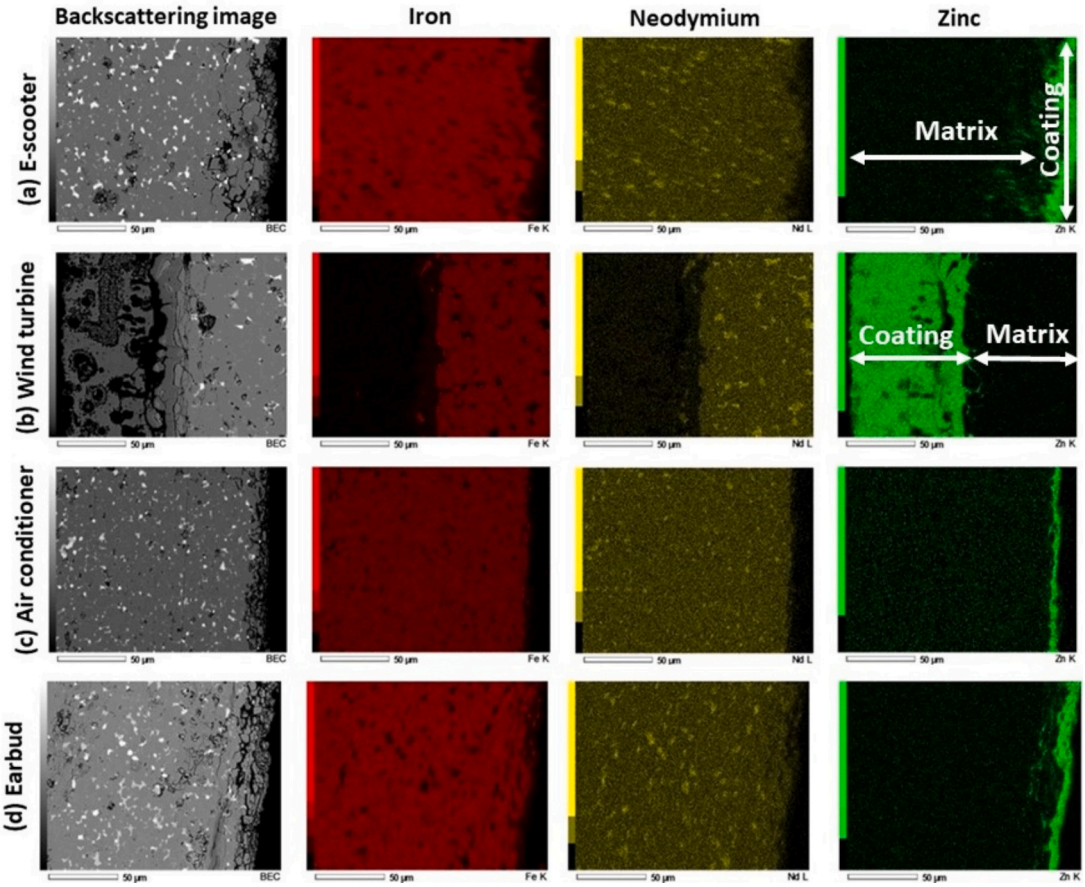

Fig. 3. Scanning backscattered images and EDS elemental mappings for Fe, Nd and Zn in the cross section of different end-of-life NdFeB permanents magnets: (a) *E*-scooter rotor; (b) wind turbine; (c) air-conditioner; (d) earbud.

from 2007 (Fig. 4 (c)), is about half of this thickness (≈ 10 µm). Nevertheless, the coating composition is all the same, consisting of a plated nickel layer.

Ni-Cu-Ni coating layer was also found during the characterisation of NdFeB PMs from earbuds. Fig. 5 shows the cross section of a sample from an earbud. The magnet matrix is similar to the previous samples, whereas the coating is composed of three layers with different thickness: Ni (≈ 3 µm), Cu (≈ 5 µm), and Ni (≈ 3 µm).

Based on SEM-EDS results from Fig. 2 - Fig. 5, the two predominant coating systems of the studied NdFeB PMs are Zn and Ni, with a varying thickness of the coating layer being an important aspect which may have a direct influence on differences in the dissolution time of the coating. Table 4 summarises the average thickness (in µm) of the coating layers found in Fig. 3 - Fig. 5.

The results in Table 1 show a variation in terms of thickness among the samples. On the other hand, in Table 4, the high standard deviation indicates that the thickness of the coating layer varies even within the same sample. For this reason, it is not accurate to use the thickness of the coating layer as a parameter to evaluate de-coating, though it is an important characteristic of the samples.

Based on analysis of the magnets' chemical composition and coating characterisation, it is clear that a labelling system for magnets is needed, indicating at least the type of magnet and coating [51]. This strategy could enhance the recycling rate of REEs, helping to meet the targets established by the EC related to the supply of recycled CRM.

3.4. *De-coating*

For the selective dissolution of the metallic coatings from spent NdFeB PMs, Ammonia-based solutions were chosen. A concentration of 5 M was selected based on preliminary tests. In the scope of this work, the target is the selective de-coating of the metallic coatings. Polymeric coatings, such as epoxy, which were found on selected magnets can easily degrade during the demagnetisation step. Thus, only samples from HDDs and *E*-scooters were tested for de-coating due to the availability of multiple similar samples that contain the two major coating types (Ni and Zn).

In this work, the first evaluated condition was 5 M NH_3 with 0.25 M NH_4Cl at 75 °C, and initial pH was around 12. The PM's samples from HDD (Ni coated) and E-scooter (Zn coated) used for de-coating weighted 6.19 g and 7.24 g, respectively; each experiment (one per sample) was performed with 300 mL solution. The following reactions may happen in

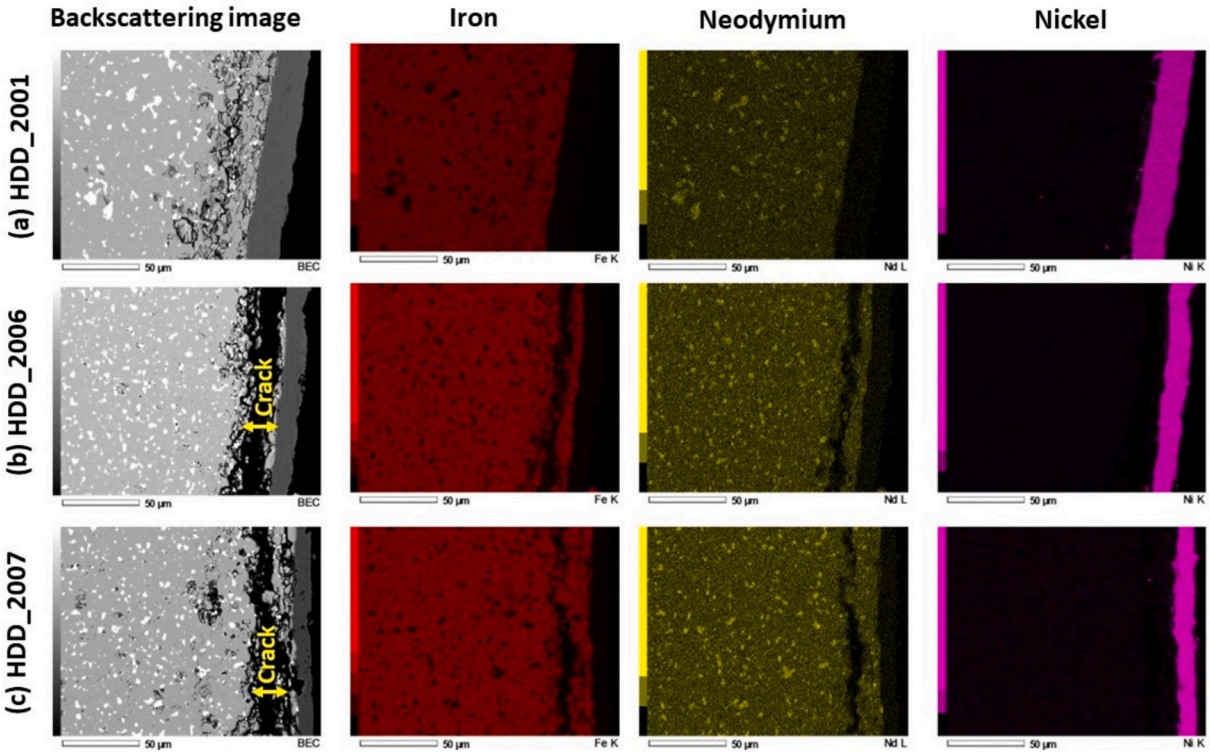

Fig. 4. Scanning backscattered images and EDS elemental mappings for Fe, Nd and Ni in the cross section of different end-of-life NdFeB permanents magnets from hard-disc drivers produced in different years: (a) 2001; (b) 2006; (c) 2007.

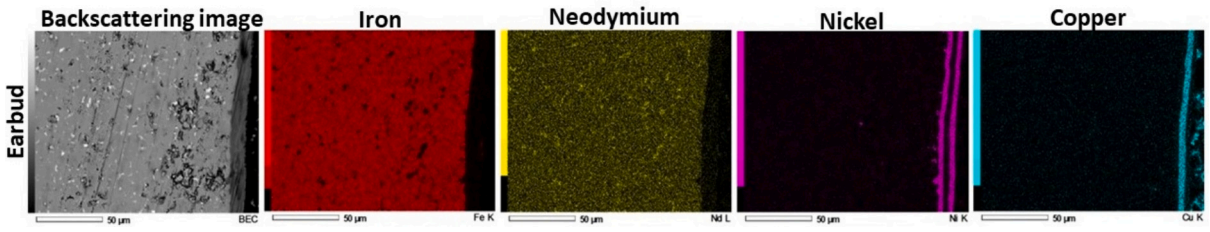

Fig. 5. Scanning backscattered image and EDS elemental mapping of the cross section of the NdFeB permanent magnet sample from earbud for Fe, Nd, Ni and Cu.

Table 4
- Average coating thickness present on different end-of-life NdFeB permanent magnets, based on the SEM-EDS analyses from Fig. 3 to Fig. 5.

PM sample	Metallic coating	Average thickness (µm)	Standard deviation
E-scooter	Zn	14.0	2.9
Wind turbine	Zn	82.0	2.4
Air conditioner	Zn	4.5	1.6
Earbud	Zn	10.0	3.2
Earbud	Ni-Cu-Ni	11.0	1.0
Hard-disc driver (year 2001)	Ni	21.0	0.7
Hard-disc driver (year 2006)	Ni	14.0	1.5
Hard-disc driver (year 2007)	Ni	11.0	1.1

this system, according to eqs. 1–3:

$$NH_3 + H_2O \rightleftharpoons NH_4OH \quad (1)$$

$$NH_4Cl \rightleftharpoons NH_3 + H^+ + Cl^- \quad (2)$$

$$NH_3 + Me \rightleftharpoons Me(NH_3)_x^{y+} + ye^- \quad (3)$$

The auto-ionization of NH_3 with water (Eq. 1) is inherent to ammonia solutions. The dissociation of the additional NH_4Cl (Eq. 2) is a key reaction to guarantee sufficient NH_3 for the complex formation (eq. 3) with Ni and Zn.

Fig. 6 shows the results of ICP-OES, in which the concentration (ppm) of metals dissolved in the system are given. The de-coating of Ni and Zn coated PMs are shown in Fig. 6 (a) and (b), respectively.

The dissolution of Ni in Fig. 6 (a) shows a gradual increment, from 4 ppm to 29 ppm in 6 h. This indicates that Ni was not removed completely, and its dissolution is time dependent; i.e., the kinetics of the system may play an important role. On the other hand, the concentration of dissolved Zn in Fig. 6(b) is higher than the Ni one, >100 ppm from the first hour. After three hours, there is a peak in the dissolution (≈130 ppm), which can be attributed to an artefact. The final concentration of Zn dissolved after 5 h is nearly the same as after just one hour. In summary, from Fig. 5 it is seen that the Zn dissolution is much faster than the Ni one. Nonetheless, the coating ratios are significantly different. For example, in the samples used for de-coating (HDD PM 6.19 g and *E*-scooter PM 7.24 g), the average contents of Ni and Zn in the magnet composition are 7 wt% and 0.4 wt% respectively (Table 3). Additionally, the average coating thicknesses is approximately 15 µm for both Ni and Zn (Table 4). Consequently, the Ni ratio is 0.03 g/µm, whereas the Zn ratio is 0.003 g/µm.

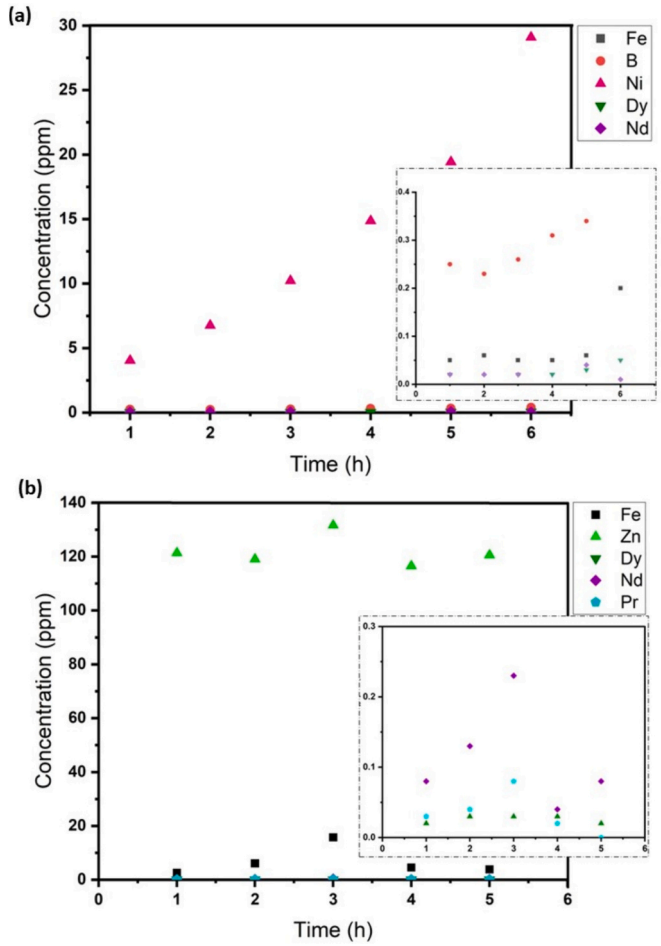

Fig. 6. Concentration of dissolved elements in the leachate analysed by ICP-OES after de-coating NdFeB PMs in 5 M NH_3 + 0.25 M NH_4Cl at 75 °C. (a) Ni-coated NdFeB PM from HDD; (b) Zn-coated NdFeB PM from *E*-scooter. The inset images in (a) and (b) highlight the low concentration from 0 up to 0.4 ppm.

Regarding the dissolution behaviour of Fe, it exhibits a similar trend to that of Zn. However, the concentration of Fe dissolved is much lower; it varied from 2 ppm to 3 ppm. This confirms the selectivity of ammonia-based solution over iron. There is also a peak of 16 ppm at 3 h, which appears to be a results of measurement artefact. It is important to highlight that the concentration of REEs dissolved was lower than 1 ppm in both case (inset Fig. 6 (a)-(b)). This indicates that NH_3-NH_4Cl medium could be used for a selective dissolution of both Ni and Zn coatings, with the advantage of not dissolving the magnet bulk. To confirm that, leaching of a PM from a HDD (2.65 g), without coating (removed manually by griding), in 300 mL of 5 M NH_3 solution (pH 12) at 75 °C was carried out for 5 h (without the addition of NH_4Cl). <0.05 ppm of Nd and 0.07 ppm of Pr was found in the resulting leachate. Additionally, the equilibrium for dissolution of REEs in NH_3 was evaluated by analysing the E-pH diagram of Nd in NH_3, as seen in Fig. 7. Fig. 7 (a) represents the E-pH diagram of Nd in 1 M NH_3 at 25 °C, while Fig. 7 (b) shows the E-pH diagram of Nd in 5 M NH_3 at 75 °C. It is expected that other REEs, such as Dy and Pr, will have similar behaviour as Nd [11].

The main difference between Fig. 7 (a) and (b) is the possible formation of NdO_2^- at high pH (>13.25). From different simulations of the *E*-pH diagrams, it was noticed that the formation of this compound is influenced exclusively by temperature. In general, NdO^+ is the predominant compound, and it is influenced by changing the NH_3 concentration and temperature. In Fig. 7 (b), the condition in which the leaching was carried out, the NdO^+ is stable in a large range of pH (≈ 3.75–12.5), and in potentials higher than −1.2 V. However, at pH slightly higher than 12, the Nd easily passivates due to the formation of $Nd(OH)_3$. In this case, Nd dissolution is inhibited by the formation of a protective layer. This could explain the low concentration (0.05 ppm) of REEs in the leachate analysed by ICP-OES.

In addition to the low dissolution of REEs in NH_3, the Fe dissolution in this medium was also very low; its maximum concentration found by ICP-OES was 0.09 ppm. It is known that Fe passivates in alkaline media, but the presence of Cl^- may promote the breakdown of this passive layer, enhancing the Fe dissolution [52,53]. Therefore, the addition of NH_4Cl can be correlated as the reason for the dissolution of Fe, even in a low range, as seen in Fig. 6 (b). If the de-coating of Zn is an efficient procedure, the NdFeB substrate will be exposed to the medium. Conversely, the reason why Fe dissolution was not seen in Fig. 6 (a) (Ni de-coating) is probably due to the low de-coating efficiency of Ni in NH_3-NH_4Cl. In this case, the Ni layer would still protect the substrate. To confirm that, the samples' cross sections were characterised by SEM-EDS after de-coating experiments; the results are shown in Fig. 8.

Fig. 8 shows the cross sections of the PMs from a HDD and E-scooter, after de-coating. Fig. 3 (a) and Fig. 4, can be used as reference for the initial condition of the Zn and Ni coatings, respectively. Nevertheless, it is worth to note that the initial condition of the coatings from the samples which were submitted to de-coating process were not characterised and coating thickness may differ. This was done to avoid the exposure of the NdFeB substrate during de-coating experiments.

From Fig. 8 (a) a Ni coating layer (≈ 10 μm) is seen in the sample even after 6 h in NH_3-NH_4Cl solution. This confirms that Ni still plays a role of protective barrier to the substrate. Nevertheless, the darker contrast in the coating layer, mainly in comparison to the cross-sections seen in Fig. 4, may indicate of Ni oxidation. On the other hand, from Fig. 8(b) a Zn layer is not seen, which reinforces its complete dissolution in NH_3-NH_4Cl medium. Comparing the BSE image in Fig. 3 (a) and Fig. 8 (b) they seem to be very similar, and it can raise questions about whether the Zn layer was in fact dissolved. For this reason, EDS analysis was carried out and the elemental mapping is shown in Fig. 8(c). Only Fe and Nd were found in the PM sample from *E*-scooter after de-coating, and no Zn was detected.

To understand the observed de-coating results, a thermodynamic analysis of both Ni and Zn in NH_3-based solutions was evaluated by simulating their E-pH diagrams. Fig. 9 shows the E-pH diagram of Ni-NH_3 at 75 °C.

From Fig. 9 is can be observed that Ni is an amphoteric metal, with dissolution occurring in both acidic and alkaline solutions, forming $Ni(NH_3)_6^{2+}$, NiO_2^{2-} or Ni_2OH^{3+}, depending on the potential and pH. On the other hand, a protective oxide layer can also be formed in alkaline pH, causing the Ni passivation due to the formation of $Ni(OH)_2$ or, beyond the water stability, NiO*OH.

It is expect that both Ni and Zn form ammine compounds when dissolved in ammonia [40,42]. The standard electrochemical potential for the Ni oxidation into $Ni(NH_3)_6^{2+}$ at 75 °C is 1.332 V, considering the standard electrochemical reduction reaction, simulated by the HSC software, shown in Eq. 4.

$$Ni(NH_3)_6(+2a) + 2e - \rightleftharpoons Ni + 6NH_3 \qquad E = -1.332\ V \tag{4}$$

In addition to the reduction potential, the variation of Standard Gibbs energy (ΔG^o) is another important thermodynamic parameter to be evaluated (although the electrochemical potential is calculated based on the Standard Gibbs energy. For the Eq. 1, ΔG^o is 256.96 kJ; this indicates that this reduction reaction is not spontaneous. On the other hand, the reversed oxidation reaction is spontaneous. Nonetheless, the kinetics of the system must also be considered. As seen in Fig. 6 (a), the Ni dissolution rate is slow. Moreover, at positive potentials the dissolution of Ni will mostly likely to take place due to the formation of Ni_2OH^{3+} (at pH lower than 10.5).

Zn is also an amphoteric metal like Ni, as shown in *E*-pH diagram in Fig. 10. Its dissolution in ammonia forms different zinc-ammine

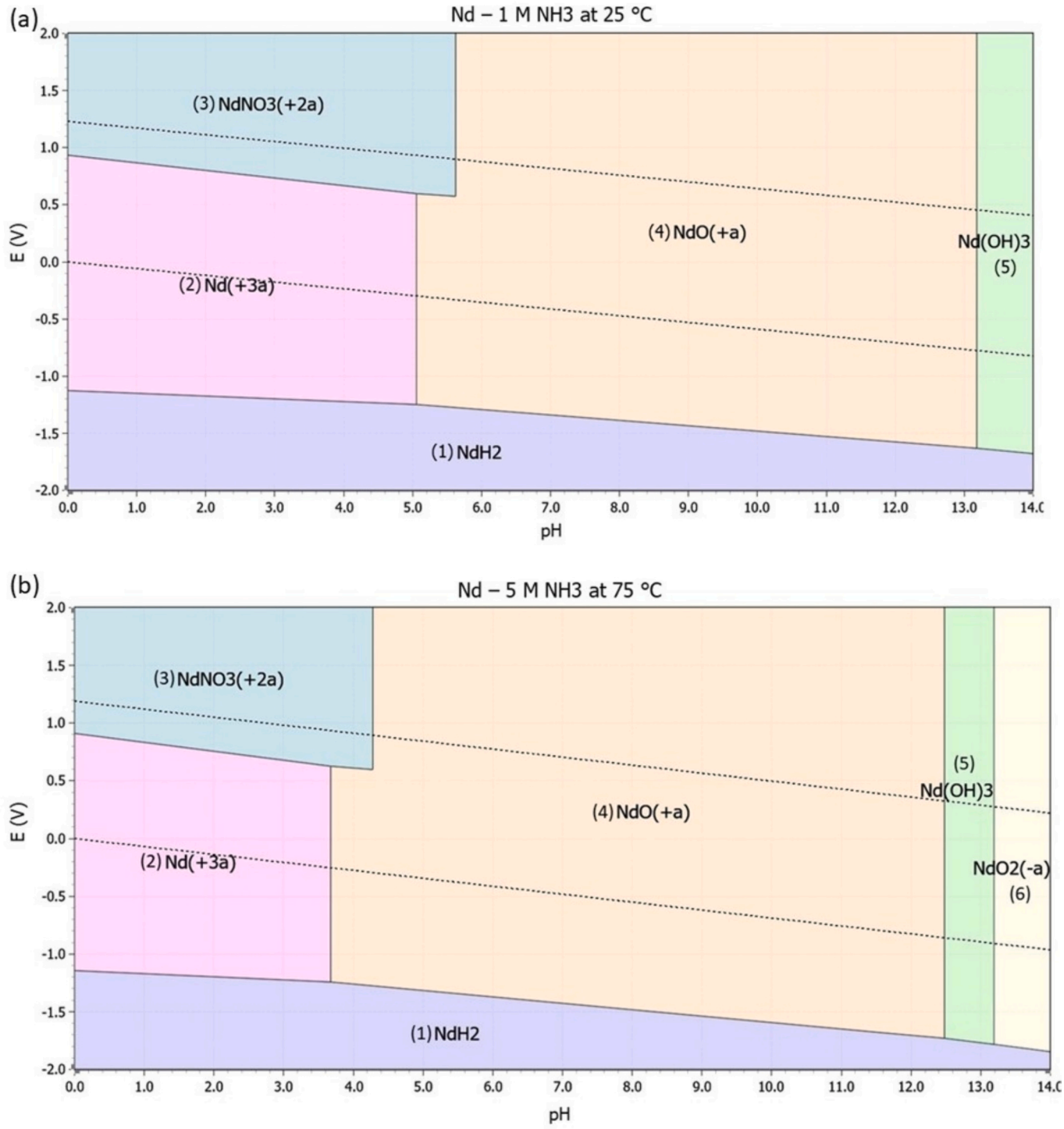

Fig. 7. *E*-pH diagrams of Nd-NH_3 in different conditions for Nd activity of 10^{-6} M: (a) 1 M NH_3 at 25 °C; (b) 5 M NH_3 at 75 °C.

compounds, depending on pH and potential. At pH 12 either $Zn(NH_3)_4^{2+}$ or $Zn(OH)_4^{2-}$ can be formed, depending on the potential.

The standard electrochemical potential for Zn oxidation into Zn $(NH_3)_4^{2+}$ at 75 °C is 1.516, considering the standard electrochemical reduction reaction shown in Eq. 5. In addition to that, the standard ΔG^o for Zn oxidation (dissolution), and formation of $Zn(NH_3)_4^{2+}$ is −292.351 kJ. Based on oxidation ΔG^o values, the formation of $Zn(NH_3)_4^{2+}$ is slightly more favourable than the formation of $Ni(NH_3)_6^{2+}$. Moreover, as shown in Fig. 9, Ni can be more prone to passivate than Zn, i.e. to form a protective oxide layer, in alkaline pH.

$$Zn(NH_3)_4(+2a) + 2e - \rightleftharpoons Zn + 4NH_3 \qquad E = -1.516\ V \tag{5}$$

Based on the thermodynamic evaluation of the Ni-NH_3 system (Fig. 9), at positive electrochemical potentials, the pH must drop to nearly 9 to dissolve the Ni in NH_3 solution. Thus, the second condition evaluated was 5 M NH_3 with addition of HCl (37 wt%) to decrease the solution to pH 9. The de-coating experiments for PM samples coated with either Ni (6.67 g) or Zn (7.24 g) were done at 75 °C for 6 h. For this condition, 300 mL of solution was also used in each experiment. The results of ICP-OES indicated that the dissolution of both Ni and Zn was

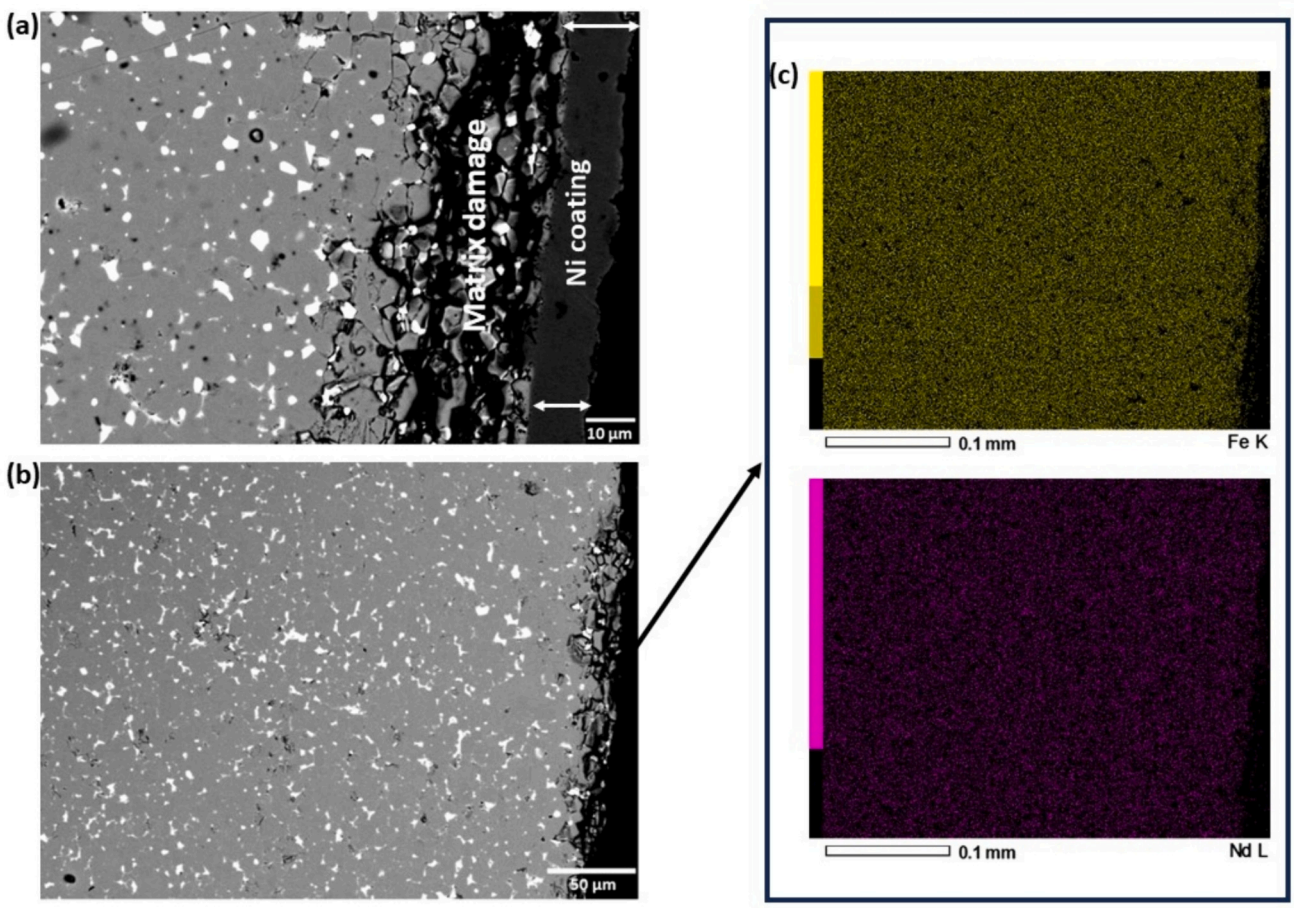

Fig. 8. Scanning backscattered images from the cross-sections of NdFeB PMs after de-coating in 5 M NH_3 + 0.25 M NH_4Cl at 75 °C: (a) Ni-coated PM sample from HDD; (b) Zn-coated PM sample from *E*-scooter; (c) EDS mapping of Fe and Nd for the cross-section image (b).

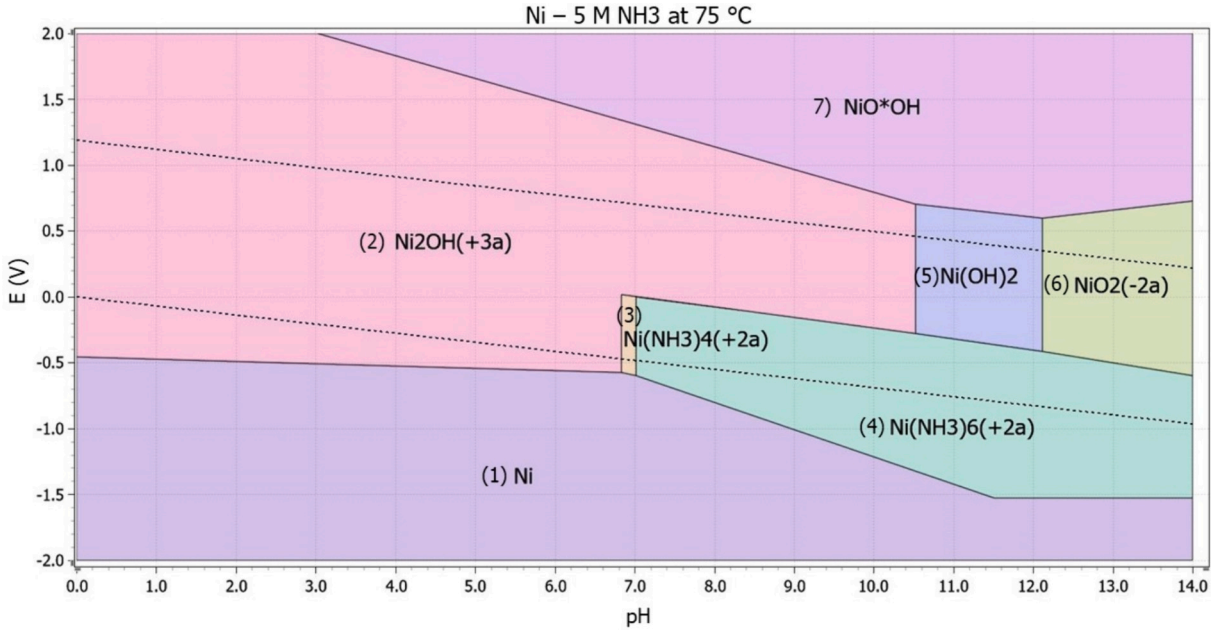

Fig. 9. E-pH diagram of Ni-NH_3 at 75 °C, considering 5 M NH_3 and Ni activity of 10^{-6} M.

even lower than the first system evaluated (NH_3-NH_4Cl, Fig. 6). The concentration of Ni dissolved in the leachate increased from 1.6 ppm (after 1 h) to 4.8 ppm (after 1 h for both cases), whereas for Zn, its concentration varied slightly over the whole experiment, in an average of 10 ppm every hour measured. Furthermore, the addition of HCl did not influence the dissolution of REEs. In other words, REEs were not

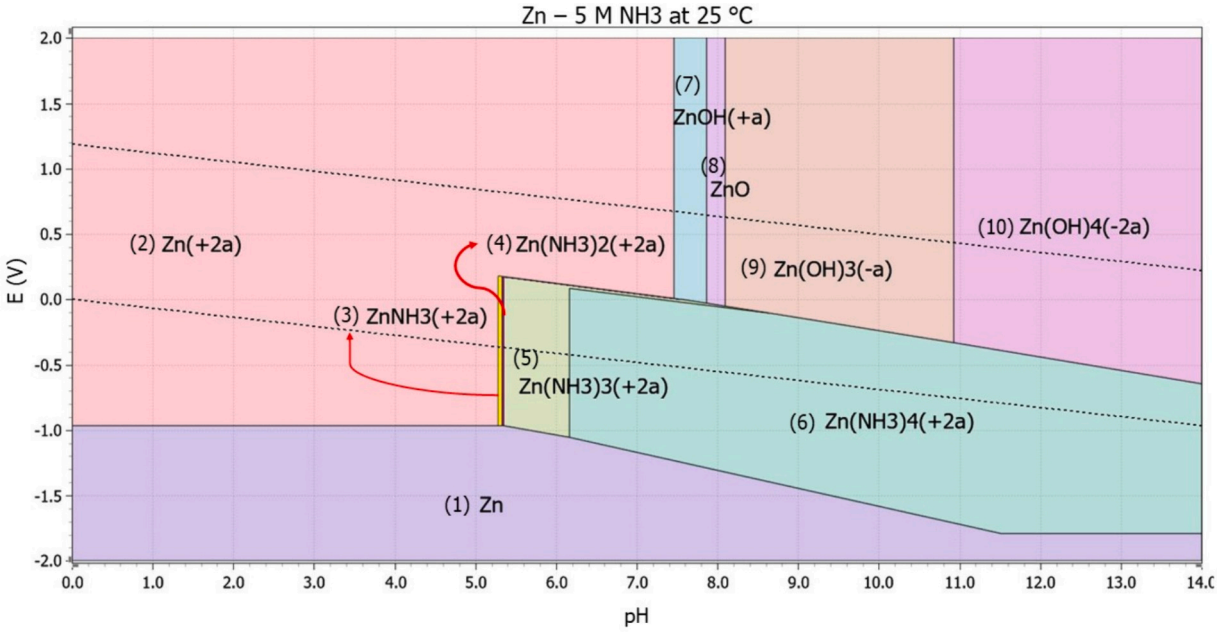

Fig. 10. E-pH diagram of Zn-NH3 at 75 °C, considering 5 M NH3 and Zn activity of 10^{-6} M.

detected in the ICP-OES results. The samples used for de-coating in NH_3 with addition of HCl were characterised by XRF before and after the leaching. The results are shown in Table 5.

As seen in Table 5, there was no significant change in the composition of the PM sample from a HDD, indicating the low efficiency of this medium for the de-coating of Ni. On the other hand, the Zn content significantly decreased after de-coating in NH_3-HCl from 74.4 to 3.9 wt %, resulting in an estimated 95% reduction. These results also suggest that the addition of NH_4Cl enhances the dissolution of Ni and Zn, as seen in Fig. 5. In other words, the concentration of both Ni and mainly Zn dissolved within time is higher in the presence of NH_4Cl. NH_4Cl may influence the equilibrium of the system and consequently, the formation of ammonia-based compound, such as $Ni(NH_3)_6^{+2}$ and $Zn(NH_3)_4^{+2}$.

The use of ammonia-based solutions for Ni leaching is a well stablished practice [40,41,43,44]. As an example, Ni recently has become a targeted element to be recovery from spent batteries due to its classification as a strategic CRM by the EU [1,44]. Wang et al. [44] have reached high Ni leaching efficiency (≈ 90%) using NH_3-$(NH_4)_2SO_4$-Na_2SO_3, where Na_2SO_3 was added as a reducing agent. However, in this condition, Ni is already in its oxidised state. The same occurs for the leaching of Ni from ores or matte. Conversely, in the de-coating experiments, it is the Ni in its metallic form aimed for dissolution. Although it is expected that the formation of stable $Ni(NH_3)_x^{y+}$ complexes increases the solubility of Ni metal in ammonia-based solutions, an oxidant agent should be considered to enhance this solubility [40].

An additional Ni de-coating experiment was done in which H_2O_2 (10% *v*/v) was added in 5 M ammonia solution. The results can be found in the Supplementary data (Table S2). In summary, very little Ni dissolution (0.7 ppm) started only after two hours of exposure to ammonia with H_2O_2. Furthermore, the concentration of Ni dissolved was periodically increasing and decreasing within time. The pH was also monitored during the experiment, but it did not vary substantially (from 10.3 to 9.9). Therefore, this variation in the concentration of Ni dissolved cannot be attributed clearly to the pH effect, due to small difference. The concentration of Ni dissolved after 6 h was just 0.2 ppm. Probably, the addition of H_2O_2 promoted the passivation of Ni instead of its oxidation.

The use of ammonia-based solutions, mainly the NH_3-NH_4Cl system, was shown thermodynamically suitable to selectively dissolve both Ni and Zn coating layers from NdFeB PM, while preserving the bulk magnet. However, the results showed that kinetics plays an important role on the dissolution process, showing that the Zn dissolution is faster and more efficient than the Ni coating. Finally, coating removal from NdFeB PMs using ammonia media, could enhance the purity of recycled magnets by direct recycling methods, especially considering Zn contamination. However, further investigations of the oxidation level, and carbon content in the magnets after complete de-coating have to be considered, as studies have shown their detrimental influence non the magnets properties [23,29,54].

4. Conclusion

Samples NdFeB PMs from different EoL products were characterised. Critical and practical aspects from disassembling to the de-coating were highlighted, with the main findings summarised as follows:

i. A challenge for the disassembly and de-coating processes is that magnets from EoL products have different sizes, weights, and their composition (considering both bulk and coating) is not known beforehand. This increases the complexity to design a universal (automated) pre-processing suitable for the different EoL products.

Table 5
- Samples' surface characterisation by XRF showing the elemental composition (wt%), before and after de-coating in 5 M NH_3 + HCl.

Sample	Coating	Condition	Ni	Zn	Fe	Nd	Pr	Dy
HDD	Ni	Before de-coating	96.9	–	2.2	0.5	0.1	–
HDD	Ni	After de-coating	96.0	–	2.9	0.6	0.1	–
E-Scooter	Zn	Before de-coating	–	74.4	16.0	7.0	n.d.	1.8
E-Scooter	Zn	After de-coating	–	3.9	63.9	18.2	4.9	n.d*.

* n.d. - not detected.

ii. Dismantling is the most effective way to obtain high-grade PM scrap for direct recycling. However, small magnets such as the ones in earbuds, cannot be easily liberated and produce too little yield to justify the efforts.
iii. In the scope of this work, Ni, Zn, Ni-Cu-Ni and epoxy were the coating systems found in the investigated EoL products. All the samples from HDDs were found to be coated with Ni, whereas all samples from *E*-scooter were coated with Zn.
iv. The thickness of the coating layer is not an accurate parameter to evaluate its dissolution, as it varies among magnet samples, and even within one magnet. This becomes an issue mainly for spent PMs from different sources, because they have different size, weight and depending on their applications the coating layer may be thicker or thinner.
v. The use of ammonia-based solutions was shown as a suitable medium to selectively dissolve both Ni and Zn coating layers from NdFeB PMs, while preserving the bulk magnet. However, only Zn was successfully dissolved, approximately 95%, while Ni dissolution was too slow despite thermodynamic predictions, making the process impractical.

CRediT authorship contribution statement

Camila Pucci Couto: Writing – review & editing, Writing – original draft, Visualization, Methodology, Investigation, Conceptualization. **Johannes J.M.M. van de Ven:** Writing – review & editing. **Yongxiang Yang:** Writing – review & editing, Visualization, Validation. **Shoshan T. Abrahami:** Writing – review & editing, Visualization, Validation, Supervision, Project administration, Methodology.

Declaration of competing interest

The authors declare that they have no known competing financial interests or personal relationships that could have appeared to influence the work reported in this paper.

Data availability

The raw/processed data required to reproduce these findings can be shared upon request.

Acknowledgments

The authors would like to thank Ruud Hendrikx at the Department of Materials Science and Engineering of the Delft University of Technology for the XRF analysis, and the companies SUEZ and CRM for the spent magnets received.

Appendix A. Supplementary data

Supplementary data to this article can be found online at https://doi.org/10.1016/j.susmat.2024.e01041.

References

[1] European Commission, Study on the Critical Raw Materials for the EU, 2023, https://doi.org/10.2873/725585.
[2] European Commission, Press Release Critical Raw Materials: Ensuring Secure and Sustainable Supply Chains for EU's Green and Digital Future, 2023.
[3] K. Binnemans, P.T. Jones, B. Blanpain, T. Van Gerven, Y. Yang, A. Walton, M. Buchert, Recycling of rare earths: a critical review, J. Clean. Prod. 51 (2013) 1–22, https://doi.org/10.1016/j.jclepro.2012.12.037.
[4] M.V. Reimer, H.Y. Schenk-Mathes, M.F. Hoffmann, T. Elwert, Recycling decisions in 2020, 2030, and 2040—when can substantial NdFeB extraction be expected in the EU? Metals (Basel). 8 (2018) https://doi.org/10.3390/met8110867.
[5] Q. Liu, K. Sun, X. Ouyang, B. Sen, L. Liu, T. Dai, G. Liu, Tracking three decades of global neodymium stocks and flows with a trade-linked multiregional material flow analysis, Environ. Sci. Technol. 56 (2022) 11807–11817, https://doi.org/10.1021/acs.est.2c02247.
[6] Y. Yang, A. Walton, R. Sheridan, K. Güth, R. Gauß, O. Gutfleisch, M. Buchert, B. M. Steenari, T. Van Gerven, P.T. Jones, K. Binnemans, REE recovery from end-of-life NdFeB permanent magnet scrap: a critical review, J. Sustain. Metall. 3 (2017) 122–149, https://doi.org/10.1007/s40831-016-0090-4.
[7] S.T. Abrahami, Y. Xiao, Y. Yang, Rare-earth elements recovery from post-consumer hard-disc drives, trans. Institutions min. Metall. Sect. C miner. Process. Extr, Metall 124 (2015) 106–115, https://doi.org/10.1179/1743285514Y.0000000084.
[8] F. Coelho, S. Abrahami, Y. Yang, B. Sprecher, Z. Li, N.-E. Menad, K. Bru, T. Marcon, C. Rado, B. Saje, M.-L. Sablayrolles, V. Decottignies, Upscaling of permanent magnet dismantling and recycling through VALOMAG project, Int. Conf. Raw Mater. Circ. Econ., MDPI, Basel Switzerland, 2021, p. 74, https://doi.org/10.3390/materproc2021005074.
[9] E. Alonso, A.M. Sherman, T.J. Wallington, M.P. Everson, F.R. Field, R. Roth, R. E. Kirchain, Erratum: Evaluating rare earth element availability: A case with revolutionary demand from clean technologies (Environmental Science and Technology (2012) 46:6 (3406–3414) DOI: 10.1021/es203518d), Environ. Sci. Technol. 46 (2012) 4684, https://doi.org/10.1021/es3011354.
[10] The Global Rare Earth Industry Association, Rare Earths. https://global-reia.org/rare-earth/ (accessed May 7, 2024).
[11] S. Belfqueh, A. Seron, S. Chapron, G. Arrachart, N. Menad, Evaluating organic acids as alternative leaching reagents for rare earth elements recovery from NdFeB magnets, J. Rare Earths (2022), https://doi.org/10.1016/j.jre.2022.04.027.
[12] P. Venkatesan, T. Vander Hoogerstraete, T. Hennebel, K. Binnemans, J. Sietsma, Y. Yang, Selective electrochemical extraction of REEs from NdFeB magnet waste at room temperature, Green Chem. 20 (2018) 1065–1073, https://doi.org/10.1039/C7GC03296J.
[13] A. Kumari, N.S. Dipali, S.K. Sahu Randhawa, Electrochemical treatment of spent NdFeB magnet in organic acid for recovery of rare earths and other metal values, J. Clean. Prod. 309 (2021) 127393, https://doi.org/10.1016/j.jclepro.2021.127393.
[14] I. Makarova, E. Soboleva, M. Osipenko, I. Kurilo, M. Laatikainen, E. Repo, Electrochemical leaching of rare-earth elements from spent NdFeB magnets, Hydrometallurgy 192 (2020) 105264, https://doi.org/10.1016/j.hydromet.2020.105264.
[15] A. Walton, H. Yi, N.A. Rowson, J.D. Speight, V.S.J. Mann, R.S. Sheridan, A. Bradshaw, I.R. Harris, A.J. Williams, The use of hydrogen to separate and recycle neodymium-iron-boron-type magnets from electronic waste, J. Clean. Prod. 104 (2015) 236–241, https://doi.org/10.1016/j.jclepro.2015.05.033.
[16] C. Jönsson, M. Awais, L. Pickering, M. Degri, W. Zhou, A. Bradshaw, R. Sheridan, V. Mann, A. Walton, The extraction of NdFeB magnets from automotive scrap rotors using hydrogen, J. Clean. Prod. 277 (2020), https://doi.org/10.1016/j.jclepro.2020.124058.
[17] R.T. Stein, A.C. Kasper, H.M. Veit, Recovery of rare earth elements present in Mobile phone magnets with the use of organic acids, Minerals 12 (2022), https://doi.org/10.3390/min12060668.
[18] A. Dańczak, I. Chojnacka, S. Matuska, K. Marcola, A. Leśniewicz, M. Wełna, A. Zak, Z. Adamski, L. Rycerz, The recycling-oriented material characterization of hard disk drives with special emphasis on NdFeB magnets, Physicochem. Probl. Miner. Process. 54 (2018) 363–376, https://doi.org/10.5277/ppmp1843.
[19] Y. Yang, S. Abrahami, Y. Xiao, Recovery of rare earth elements from Eol permanent magnets with slag extraction, 3rd Int. Slag Valoris, Symp., Leuven, 2013, pp. 249–252.
[20] T. Elwert, D. Goldmann, F. Roemer, S. Schwarz, Recycling of NdFeB magnets from electric drive motors of (hybrid) electric vehicles, J. Sustain. Metall. 3 (2017) 108–121, https://doi.org/10.1007/s40831-016-0085-1.
[21] A. Kumari, S. Kumar Sahu, A comprehensive review on recycling of critical raw materials from spent neodymium iron boron (NdFeB) magnet, Sep. Purif. Technol. 317 (2023) 123527, https://doi.org/10.1016/j.seppur.2023.123527.
[22] P. Venkatesan, Z.H.I. Sun, J. Sietsma, Y. Yang, An environmentally friendly electro-oxidative approach to recover valuable elements from NdFeB magnet waste, Sep. Purif. Technol. 191 (2018) 384–391, https://doi.org/10.1016/j.seppur.2017.09.053.
[23] C. Burkhardt, S. van Nielen, M. Awais, F. Bartolozzi, J. Blomgren, P. Ortiz, M. B. Xicotencatl, M. Degri, S. Nayebossadri, A. Walton, An overview of hydrogen assisted (direct) recycling of rare earth permanent magnets, J. Magn. Magn. Mater. 588 (2023) 171475, https://doi.org/10.1016/j.jmmm.2023.171475.
[24] V. Kaplan, Y. Feldman, K. Gartsman, G. Leitus, E. Wachtel, I. Lubomirsky, Electrolytic hydrogen Decrepitation of NdFeB magnets under ambient conditions, J. Sustain. Metall. (2022), https://doi.org/10.1007/s40831-022-00574-0.
[25] M. Zakotnik, I.R. Harris, A.J. Williams, Multiple recycling of NdFeB-type sintered magnets, J. Alloys Compd. 469 (2009) 314–321, https://doi.org/10.1016/j.jallcom.2008.01.114.
[26] C. Burkhardt, A. Lehmann, P. Fleissner, L. Grau, M. Trautz, M. Mungenast, B. Podmiljšak, S. Kobe, Comparative evaluation of anti-corrosion coatings for NdFeB-type magnets with respect to performance and recyclability via hydrogen-assisted recycling (HPMS), Mater. Proc. 5 (2021) 87, https://doi.org/10.3390/materproc2021005087.
[27] C.A.L. dos Santos, Z. Panossian, Permanent rare-earth magnets—the need to protect them against corrosion, Mater. Sci. Appl. 10 (2019) 317–327, https://doi.org/10.4236/msa.2019.104024.
[28] M. Orefice, A. Eldosouky, I. Škulj, K. Binnemans, Removal of metallic coatings from rare-earth permanent magnets by solutions of bromine in organic solvents, RSC Adv. 9 (2019) 14910–14915, https://doi.org/10.1039/c9ra01696a.
[29] L. Grau, P. Fleissner, S. Kobe, C. Burkhardt, Processability and Separability of commercial anti-corrosion coatings produced by in situ hydrogen-processing of

magnetic scrap (HPMS) recycling of NdFeB, Materials (Basel). 17 (2024) 2487, https://doi.org/10.3390/ma17112487.
[30] M. Zakotnik, I.R. Harris, A.J. Williams, Possible methods of recycling NdFeB-type sintered magnets using the HD/degassing process, J. Alloys Compd. 450 (2008) 525–531, https://doi.org/10.1016/j.jallcom.2007.01.134.
[31] Y. Hu, M. Aindow, I.P. Jones, I.R. Harris, Effects of Zn coating on the microstructure and magnetic properties of Nd-Fe-B magnets, J. Alloys Compd. 351 (2003) 299–303, https://doi.org/10.1016/S0925-8388(02)01070-8.
[32] Y. Li, Y.B. Kim, T.S. Yoon, D.S. Suhr, T.K. Kim, C.O. Kim, Coercivity enhancement by Zn addition in hot deformed NdFeB magnets, J. Magn. Magn. Mater. 242–245 (2002) 1369–1371, https://doi.org/10.1016/S0304-8853(01)01285-9.
[33] J. Li, C. Guo, T. Zhou, Z. Qi, X. Yu, B. Yang, M. Zhu, Effects of diffusing DyZn film on magnetic properties and thermal stability of sintered NdFeB magnets, J. Magn. Magn. Mater. 454 (2018) 215–220, https://doi.org/10.1016/j.jmmm.2018.01.070.
[34] Y.L. Ma, Y. Liu, J. Li, H.L. Du, J. Gao, Anisotropic nanocomposite Nd2Fe14B/α-Fe magnets prepared by spark plasma sintering, IEEE Trans. Magn. 45 (2009) 2605–2607, https://doi.org/10.1109/TMAG.2009.2018911.
[35] L. Kelhar, J. Zavaśnik, P. McGuiness, S. Kobe, The impact of processing parameters on the properties of Zn-bonded Nd-Fe-B magnets, J. Magn. Magn. Mater. 419 (2016) 171–175, https://doi.org/10.1016/j.jmmm.2016.06.035.
[36] Y. Hu, I.R. Harris, M. Aindow, I.P. Jones, Defect formation in Nd2Fe14B grains caused by Zn diffusion, Philos. Mag. Lett. 81 (2001) 233–241, https://doi.org/10.1080/09500830010029427.
[37] M. Lv, Y. Li, T. Kong, M. Zhu, H. Jin, W. Li, Coercivity enhancement in Dy-free HDDR Nd-Fe-B powders by the grain boundary diffusion of Zn, J. Magn. Magn. Mater. 523 (2021) 167589, https://doi.org/10.1016/j.jmmm.2020.167589.
[38] T. Horikawa, M. Itoh, S. Suzuki, K. Machida, Magnetic properties of the Nd-Fe-B sintered magnet powders recovered by Yb metal vapor sorption, J. Magn. Magn. Mater. 271 (2004) 369–380, https://doi.org/10.1016/j.jmmm.2003.10.003.
[39] X.G. Cui, X.H. Wang, G.C. Yin, C.Y. Cui, C.D. Xia, T.Y. Ma, C. Wang, B.X. Peng, J. X. Pan, P. Mei, Magnetic properties and microstructure of sintered Nd–Fe–B magnets with intergranular addition of Ni powders, J. Alloys Compd. 726 (2017) 846–851, https://doi.org/10.1016/j.jallcom.2017.08.061.
[40] X. Meng, K.N. Han, The principles and applications of Ammonia leaching of metals—a review, Miner. Process. Extr. Metall. Rev. 16 (1996) 23–61, https://doi.org/10.1080/08827509608914128.
[41] K. Bhuntumkomol, K.N. Han, F. Lawson, The leaching behaviour of nickel oxides in acid and in ammoniacal solutions, Hydrometallurgy 8 (1982) 147–160, https://doi.org/10.1016/0304-386X(82)90041-X.
[42] Z. Huajun, G. Zhenghai, Z. Jinhuan, Study on the dissolution process of zinc anode in ammoniacal ammonium chloride system, Hydrometallurgy 89 (2007) 369–373, https://doi.org/10.1016/j.hydromet.2007.08.008.
[43] E. Muzenda, I.M. Ramatsa, F. Ntuli, A.S. Abdulkareem, A.S. Afolabi, Parametric effects on leaching behavior of nickel-copper matte in ammonia, Part. Sci. Technol. 31 (2013) 319–325, https://doi.org/10.1080/02726351.2012.736456.
[44] H. Wang, Z. Li, Q. Meng, J. Duan, M. Xu, Y. Lin, Y. Zhang, Ammonia leaching of valuable metals from spent lithium ion batteries in NH3-(NH4)2SO4-Na2SO3 system, Hydrometallurgy 208 (2022) 105809, https://doi.org/10.1016/j.hydromet.2021.105809.
[45] A. Verma, O.P. Pandey, P. Sharma, Strontium ferrite permanent magnet - an overview, Indian J. Eng, Mater. Sci. 7 (2000) 364–369.
[46] L. Welzel, End-of-Life Wind Turbines in the EU : An Estimation of the NdFeB-Magnets and Containing Rare Earth Elements in the Anthropogenic Stock of Germany and Denmark, Uppsala University, 2019. https://www.diva-portal.org/smash/record.jsf?dswid=-8452&pid=diva2%3A1359833&c=1&searchType=SIMPLE&language=en&query=An+Estimation+of+the+NdFeB-Magnets+and+Containing+Rare+Earth+Elements+in+the+Anthropogenic+Stock+of+Germany+and+Denmark&af=%5B%5D&aq=%5B%5B%5D%5D&aq2=%5B%5B%5D%5D&aqe=%5B%5D&noOfRows=50&sortOrder=author_sort_asc&sortOrder2=title_sort_asc&onlyFullText=false&sf=all.
[47] T. Maani, N. Mathur, C. Rong, J.W. Sutherland, Estimating potentially recoverable Nd from end-of-life (EoL) products to meet future U.S. demands, Resour. Conserv. Recycl. 190 (2023) 106864, https://doi.org/10.1016/j.resconrec.2023.106864.
[48] Y. Cao, Y. Liu, P. Zhang, G. Xu, J. Liu, J. Chen, X. Yi, Y. Wu, Corrosion resistance and mechanical properties of (Ho,Nd)FeB magnets, J. Rare Earths 39 (2021) 1409–1414, https://doi.org/10.1016/j.jre.2020.08.006.
[49] K. Ortegon, L.F. Nies, J.W. Sutherland, Preparing for end of service life of wind turbines, J. Clean. Prod. 39 (2013) 191–199, https://doi.org/10.1016/j.jclepro.2012.08.022.
[50] B.M. Durodola, J.A.O. Olugbuyiro, S.A. Moshood, O.S. Fayomi, A.P.I. Popoola, Study of influence of zinc plated mild steel deterioration in seawater environment, Int. J. Electrochem. Sci. 6 (2011) 5605–5616, https://doi.org/10.1016/s1452-3981(23)18431-8.
[51] C. Burkhardt, A. Lehmann, B. Podmiljsak, S. Kobe, A systematic classification and labelling approach to support a circular economy ecosystem for NdFeB-type magnet, J. Mater. Sci. Eng. B. 10 (2020), https://doi.org/10.17265/2161-6221/2020.7-8.001.
[52] Z. Panossian, L. Mariaca, M. Morcillo, S. Flores, J. Rocha, J.J. Peña, F. Herrera, F. Corvo, M. Sanchez, O.T. Rincon, G. Pridybailo, J. Simancas, Steel cathodic protection afforded by zinc, aluminium and zinc/aluminium alloy coatings in the atmosphere, Surf. Coat. Technol. 190 (2005) 244–248, https://doi.org/10.1016/j.surfcoat.2004.04.023.
[53] Z. Panossian, C.A.L. dos Santos, J.L. Cardoso, L.N. da Silva, R.A. Camargo, *Interpretação de curvas de polarização* (in Portuguese), INTERCORR 2014, Fortaleza - Brazil, ABRACO, 2014, pp. 1–28.
[54] A. Saguchi, K. Asabe, T. Fukuda, W. Takahashi, R.O. Suzuki, Recycling of rare earth magnet scraps: carbon and oxygen removal from Nd magnet scraps, J. Alloys Compd. 408–412 (2006) 1377–1381, https://doi.org/10.1016/j.jallcom.2005.04.178.